Energy consumption analysis of constant voltage and constant current operations in capacitive deionization

Supporting information

Yatian Qu,[a,b] *Patrick G. Campbell,*[b] *Lei Gu,*[c] *Jennifer M. Knipe,*[b] *Ella Dzenitis,*[d] *Juan G. Santiago*[a]* *and Michael Stadermann*[b]*

[a] Department of Mechanical Engineering, Stanford University Stanford, CA 94305, USA

[b] Lawrence Livermore National Laboratory, 7000 East Avenue, Livermore, CA, USA.

[c] Department of Electrical Engineering, Stanford University Stanford, CA 94305, USA

[d] Dartmouth College, Hanover, NH, 03755, USA

*To whom correspondence should be addressed. E-mails: juan.santiago@stanford.edu and stadermann2@llnl.gov

This document contains supplementary information and figures further describing our simple RC circuit model and transmission line (TL) based LTspice model; additional simulation results of constant voltage (CV) and constant current (CC) operations; and

characterization of capacitance, resistances and parasitic reactions of flow-through capacitive deionization (ftCDI) cell.

- S-1: Simulation results from a simple RC circuit
- S-2: LTSpice model description
- S-3: Cyclic voltammetry to evaluate charging capacitances
- S-4: Electrochemical impedance spectroscopy to measure resistances
- S-5: Characterization and modeling of parasitic reactions
- S-6: Comparison of input charge from experiments and simulations
- S-7: CDI cell electrode salt adsorption capacities

S-1 Simulation results from a simple RC circuit

We here further describe our simple RC circuit model of a CDI cell to compare energy consumption of CV and CC modes, as a first-order of analysis. Our experiments suggest our cell has a total resistance R of 7.64 Ω and electrical double layer capacitance C of 3.84 F. Energy consumption of CV and CC modes using the simple RC circuit are evaluated by Equation 4 and 7 in the main text, under the conditions of the same amounts of input charge and identical timespans. Figure S-1a presents simulated energy consumption with charging phase durations from 60 to 600 s, and it shows that CV consumes significantly more energy than CC, especially with longer charging times. Figure S-1b shows the simulated consumption ratios of CC to CV.

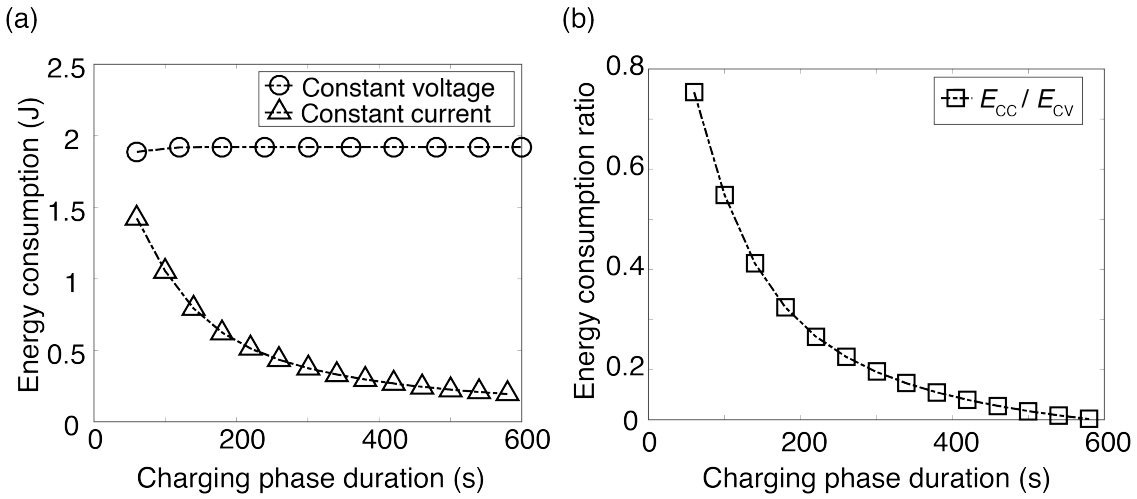

Figure S-1. a) Simulated energy consumption of a CDI cell using simple RC circuit in charging process with CV and CC modes. b) Simulated energy consumption ratio of CC to CV.

S-2 LTspice model description

We performed LTspice simulations to investigate the charging dynamics and energy consumption of a CDI cell. In our model, we have a setup resistance, a contact resistance, and two electrodes each modeled via a TL with 20 resistor-capacitor units (Figure S-2). Each resistor-capacitor unit has a value chosen to reflect the actual resistances or capacitances in our ftCDI cell. We characterized R_s, R_{ct}, and R_i from electrochemical impedance spectroscopy (EIS) data as later described in Section S-4. The characterized R_i and R_e of each electrode are related to the resistance of each element $R_{i1}, R_{i2}, \ldots R_{i19}$ and $R_{e1}, R_{e2}, \ldots R_{e20}$ as follows:

$$R_{i(j)} = R_i/N_i, \quad R_{e(k)} = R_e/N_e \quad (j=1,2, \ldots, 19; k=1,2, \ldots, 20) \tag{S1}$$

where N_i and N_e are the (arbitrarily chosen) number of elements of our discretization. We here chose N_i as 19 and N_e as 20 for each electrode.

The capacitances of each electrode C were measured by cyclic voltammetry of the whole CDI cell, as later described in Section S-3. We assume that capacitance remains constant during charging process. The capacitance of each electrode C is related to each capacitor in the circuit $C_1, C_2, \ldots C_{20}$ as follows:

$$C_{(m)} = C/N_c, \ (m=1,2, \ldots, 20) \tag{S2}$$

we here chose N_c as 20.

We model parasitic reactions of porous electrodes as non-linear resistances R_1, $R_2, \ldots R_{20}$ which follow a Bulter-Volmer equation. In LTspice, a parasitic reaction resistor is in parallel with an EDL capacitor and we used a sub-circuit to model its non-linear behavior. We describe the characterization and modeling of parasitic reactions in Section S-5.

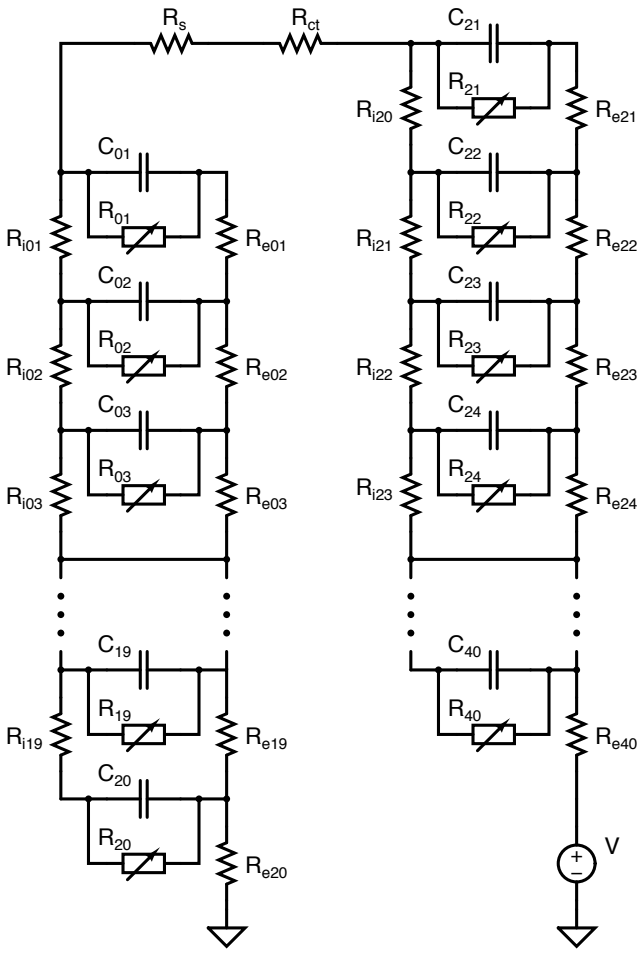

Figure S-2. Schematic of LTspice circuit model used in simulations. We discretized the electrodes using a transmission line modeling approach, and each electrode is represented by 20 resistor-capacitor units. The values of each resistor, capacitor and non-linear parasitic reaction element were determined by independent CDI cell characterization experiments to correctly reflect the properties of our CDI cell.

S-3 Cyclic voltammetry to evaluate charging capacitances

As mentioned in the main text, apparent capacitances of porous electrodes depend on charging rates.[1-3] In order to accurately assess equilibrium EDL capacitance, we performed cyclic voltammetry experiments at a slow scan rate of 1.67 mV/s. Figure S-3 shows measured differential capacitances of our ftCDI cell within a voltage window from -0.2 to 1.3 V. We averaged capacitance values from 0 to 1 V in positive sweeping phases as the capacitance inputs for LTspice models.

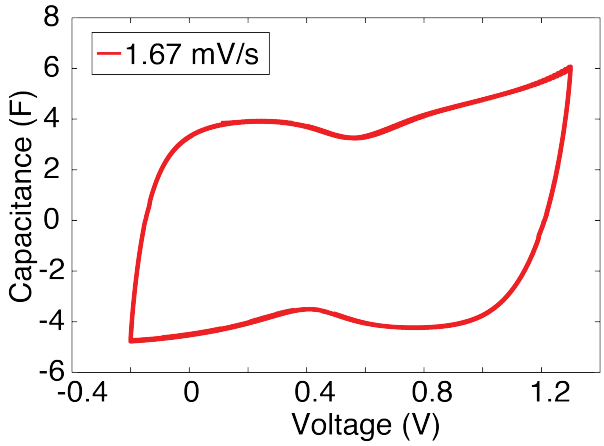

Figure S-3. Cyclic voltammetry of ftCDI cell at scan rate of 1.67 mV/s. The measurement voltage window is from -0.2 to 1.3 V.

S-4 Electrochemical impedance spectroscopy to measure resistances

We characterized resistances of our (entire assembled) ftCDI cell using electrochemical impedance spectroscopy (EIS) using a potentiostat. EIS was performed in a two-terminal configuration without a reference electrode since the electrodes of the cell were symmetric. We applied a 10 mV amplitude sinusoidal potential perturbation and scanned over a frequency range from 700 kHz to 10 mHz at 0 V bias. During electrochemical tests, the cell was filled with 100 mM NaCl. Figure S-4 shows Nyquist plot of EIS response of our ftCDI cell. We extract the values of R_s, R_{ct}, and R_i from the plot as shown in Figure S-4. [4, 5]

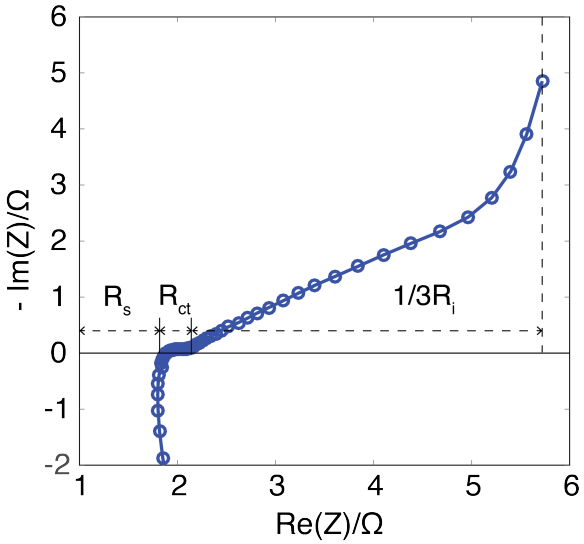

Figure S-4. Nyquist plot of ftCDI cell measured using electrochemical impedance spectroscopy for frequencies within 700 kHz to 10 mHz. The values of R_s, R_{ct}, and R_i are distances along the real axis and are denoted as the labeled line segments flanked by asterisks.

S-5 Characterization and modeling of parasitic reactions

We characterized parasitic reaction currents by performing constant voltage experiments at 0.2, 0.4, 0.6, 0.8, 1.0 and 1.2 V while flowing feed solution through the cell, and recorded leakage currents after 10 min of charging. We then fitted these leakage current data to characterize the parasitic reactions.

In our LTspice model, there are 20 leakage resistor elements in parallel with EDL capacitors for each electrode. Therefore, we divide the measured leakage currents by 20 to obtain current flowing through each resistor. These leakage currents are measured after 10 min of charging, so we can expect the voltage drops across each capacitor element (and therefore each leakage resistor element) to be approximately uniform. We therefore characterize the leakage current voltage using a single value applicable to the cell under these conditions. The voltage across a leakage resistor is obtained by subtracting an ohmic drop of setup resistance and contact resistance from cell voltage and then dividing this by two, as shown in Equation S3.

$$V_{leak} = ½ (V_{cell} - I_{cell} (R_s + R_{ct})) \quad \text{(S3)}$$

We fit parasitic currents data to characterize its voltage dependence. First, we assume that there is a turn-on voltage for parasitic reactions and we define it as V_o. We also assume that, below threshold voltage V_o, the leakage resistor behaves as a large constant resistor with a value of 50 kΩ. When the voltage is above threshold, the leakage resistor behaves non-linearly and follows Bulter-Volmer equation. Equation S4 shows the fit:

$$I_{leak} = \frac{V_0}{50k} e^{\left(\alpha(-V_0+V)\right)} \quad \text{(S4)}$$

We obtained fitting parameters V_o as 0.145 V and α as 7.12 (1/V). In implementing this relation into the model for CDI cell operation, the variable V is then the local, element-specific voltage for each leakage resistor element. We note here that we adopt a modified version of Bulter-Volmer equation because as we found it to be compatible with subcircuit implementation and solutions performed using LTspice.

Our parasitic reaction model has a Tafel slope as 320 mV/decade. In literature, oxygen reduction is usually reported to have two Tafel slopes, 60 mV/decade or 120 mV/decade, depending on the electrode materials and on the potential range.[6]. Our Tafel slope indicates slower kinetics than reported numbers. Our value is reasonable because carbon electrode is a low efficient catalyst for oxygen reduction reaction, and oxygen reduction is only one of the possible parasitic reactions. Carbon oxidation in CDI is a complicated electrochemical process and the reaction kinetics is not well studied in literature. Despite the limited data available, our fitted parameters are comparable to those reported in porous carbon supercapacitor literature.[7]

Figure S-5a shows a comparison between experimental data and our leakage resistor element model. Here, the current is the parasitic current through each leakage resistor and voltage is the voltage across one electrode (from the leakage current experiments). Figure S-5b compares simulated total parasitic currents from LTspice model after implementing non-linear leakage resistor to experimental data. The simulation data agree well with experimental data, which validates the fitting procedures.

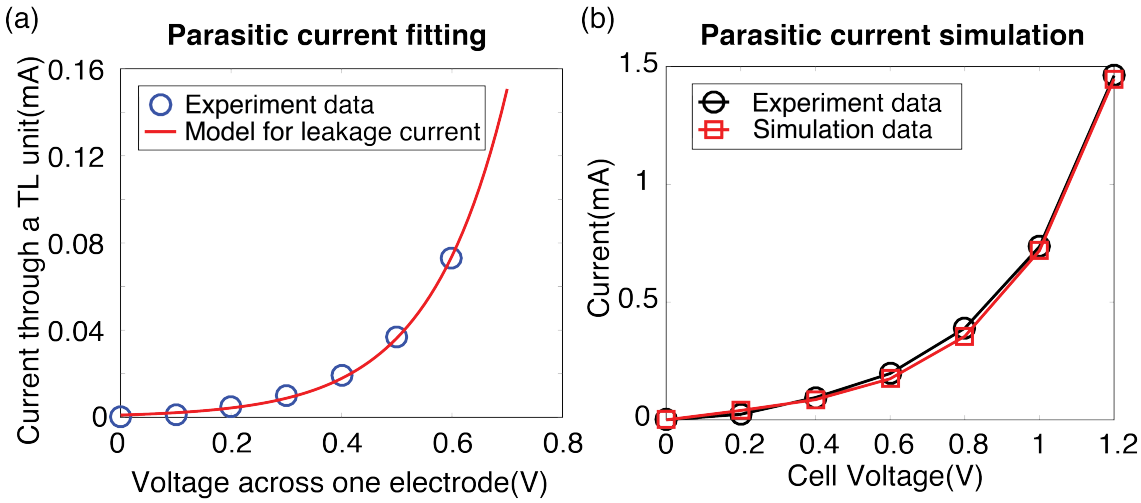

Figure S-5. a) Fitting experiment data with Bulter-Volmer equation to characterize parasitic current through each leakage resistor element. Blue circles are experimental data and the red line represents the model for leakage current. b) Parasitic currents of the whole CDI cell simulated by LTspice model after implementing non-linear leakage resistors. The simulation data agree well with experimental data.

S-6 Comparison of input charge from experiments and simulations

Figure S-6 shows the comparison of input charge from experimental data and simulation results. Simulations consistently predict higher input charges than experiments because the model does not capture the dynamic changes of ionic resistances during desalination (particularly important for constant voltage operation for short duration times). Note that CC simulations use input current from experiments and so charge transferred matches exactly with experiments.

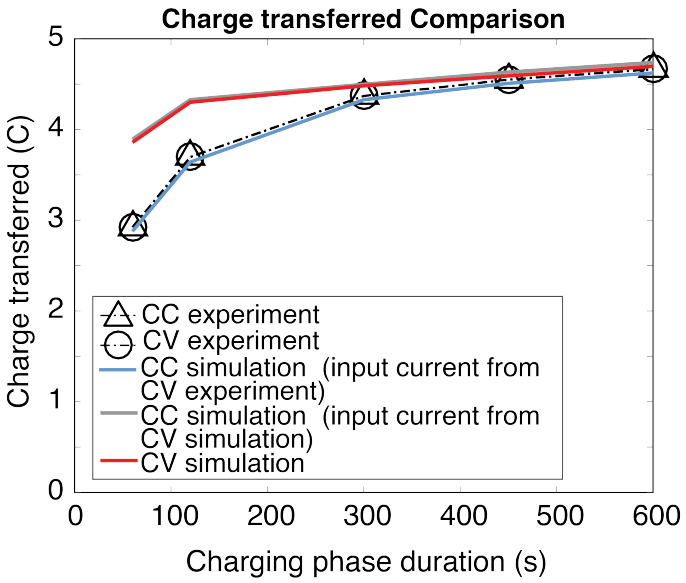

Figure S-6. Charge transfer comparison of experimental and simulation results of a ftCDI cell in CV or CC mode with charging times of 1, 2, 5, 7.5 and 10 min. CV and CC modes were operated under the conditions of the same input charges and identical charging phase timespans.

S-7 CDI cell electrode salt adsorption capacities

Figure S-7 shows the absolute salt adsorption capacities (in mg NaCl per g aerogel) of CV and CC modes with charging phase durations of 1, 2, 5, 7.5 and 10 min. The data presented here correspond to the data shown in Figure 4 in the main text. Within our ability to quantify this quantity, we observed no significance difference in salt absorption for the CC and CV modes.

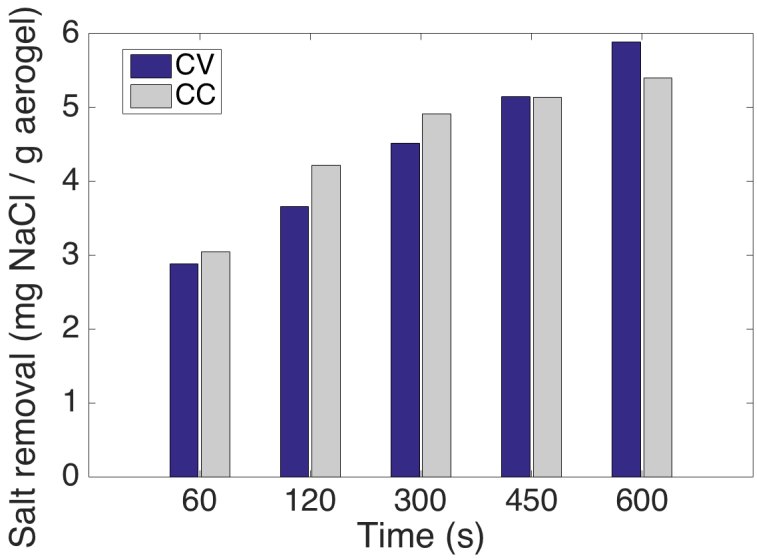

Figure S-7. Salt adsorption capacities of CV and CC modes (in mg NaCl per g aerogel) with charging phase durations of 1, 2, 5, 7.5 and 10 min.

REFERENCES

[1] M.D. Stoller, R.S. Ruoff, Best practice methods for determining an electrode material's performance for ultracapacitors, Energy & Environmental Science, 3 (2010) 1294.

[2] H. Wang, L. Pilon, Physical interpretation of cyclic voltammetry for measuring electric double layer capacitances, Electrochimica Acta, 64 (2012) 130-139.

[3] H. Wang, A. Thiele, L. Pilon, Simulations of Cyclic Voltammetry for Electric Double Layers in Asymmetric Electrolytes: A Generalized Modified Poisson–Nernst–Planck Model, The Journal of Physical Chemistry C, 117 (2013) 18286-18297.

[4] Y. Qu, T.F. Baumann, J.G. Santiago, M. Stadermann, Characterization of Resistances of a Capacitive Deionization System, Environ Sci Technol, 49 (2015) 9699-9706.

[5] M.E. Suss, T.F. Baumann, M.A. Worsley, K.A. Rose, T.F. Jaramillo, M. Stadermann, J.G. Santiago, Impedance-based study of capacitive porous carbon electrodes with hierarchical and bimodal porosity, Journal of Power Sources, 241 (2013) 266-273.

[6] Chaojie Song, J. Zhang, PEM Fuel Cell Electrocatalysts and Catalyst Layers: Fundamentals and Applications, in, Springer, 2008, pp. 89-134.

[7] T. Tevi, A. Takshi, Modeling and simulation study of the self-discharge in supercapacitors in presence of a blocking layer, Journal of Power Sources, 273 (2015) 857-862.